Tomas Bata University in Zlín
Library

Development and analyses of a lever system for a newly designed self-equalising thrust bearing

Citation

DOI

Permanent link

https://publikace.k.utb.cz/handle/10563/1010924

TBU Publications
Repository of TBU Publications
publikace.k.utb.cz

Development and analyses of a lever system for a newly designed self-equalising thrust bearing

Katarina Monkova[a,b'*]**, Marek Urban** [c]**, Stefan Moravka** [d]**, Peter Pavol Monka**[a,b]**, Željko Božić**[e]

[a] *Technical University of Kosice, Faculty of Manufacturing Technologies with the Seat in Presov Sturova 31, 080 01 Presov, Slovakia*

[b] *Tomas Bata University in Zlin, Faculty of Technology, Vavreckova 275, 760 01 Zlin, Czech Republic*

[c] *GTW Bearings s.r.o, Prisov 24, 330 11 Tremosna, Czech Republic*

[d] *New Technologies Research Center at West Bohemia University in Pilsen, Univerzitni 22, 301 00 Pilsen, Czech Republic*

[e] *University of Zagreb, Faculty of Mechanical Engineering and Naval Architecture, I. Lucica 5, 10000 Zagreb, Croatia*

* *Corresponding author at: Technical University of Kosice, Faculty of Manufacturing Technologies with the Seat in Presov Sturova 31, 080 01 Presov, Slovakia, Tomas Bata University in Žlin, Faculty of Technology, Vavreckova 275, 760 01 Žlin, Czech Republic. E-mail address: katarina.monkova@tuke.sk (K. Monkova).*

ABSTRACT

Thrust bearings are undoubtedly one of the essential parts of turbines and compressors. However, there are many cases in which asymmetric load occurs on the bearings due to e.g. thermal deformations, production inaccuracies or a simple deflection of the shaft. The presented research deals with some basic steps involved in comprehensive research related to developing a new self-equalising thrust bearing. It focuses on the design of its most crucial part - lever, which is responsible for the proper equalising functionality. The study aimed to design a new type of lever geometry, create its numerical model, and, through numerical analysis and calculations, predict its useability in real conditions. According to von Mises hypothesis, stresses were evaluated, as well as contacts and stiffness according to Hertz's theory. The lever was modelled in two sizes, which suit the bearings representing the most often used types in powerful machines. For the levers' design and production, the steel 34CrNiMo6 has been used in a refined state with a yield strength of 900 MPa. The results achieved within the experimental static tests and verifications in operating conditions confirmed the correctness of the final geometry design of the levers, its sufficient stiffness, as well as good functionality of the thrust bearing and its reliability.

Keywords: Lever, Design, Thrust bearing Analysis, Experimental tests

1. Introduction

Operating speeds, loads, and temperatures are constantly increasing in large power plant rotating machines (such as a turbine or a compressor), which places high demands on the reliability and service life of the energetic devices. One of the most stressed components, whose service life is particularly limited, is undoubtedly the thrust bearing. However, there are many cases where the bearings are loaded asymmetrically due to, e.g. thermal deformations, production inaccuracies or simple shaft deflection of the shaft. Asymmetrical loading means misalignment of the rotor with respect to the stator at an angle of more than a few tenths of a degree. This phenomenon affects the durability and safe operability of plain and thrust bearings.

Many researchers dealt with misalignment in their studies. Patel [1] used the experimental approach for the first time to determine the magnitude and harmonic nature of the misalignment excitation. The force vector is used for the misalignment coupling stiffness matrix, derived from the experimental data, and the misalignment coupling stiffness rotor is applied. Alok et al. [2] used stator current signature to diagnose misalignment. It is found that misalignment is responsible for the cause of instability. Hariharan [3] used experiments and ANSYS analysis to study the shaft misalignment. It is found that the misalignment effect can be amplified when the running speed is close to the system of natural frequency. Umbrajkaar [4] used the Lagrange approach to derive the misalignment equation, while the Newton-Raphson method was obtained from the dimensionless form. A discrete wavelet transform is used to analyse the signal. Wang et al. [5] studied the dual-rotor system with unbalance-misalignment coupling faults from simulation and experiments. Prabhakar et al. [6] analysed the transient response of a misalignment rotor-coupling-bearing system passing through the critical speed. The continuous wavelet transform has been used to extract the silent features. Saavedra and Ramirez [7] deduced a new coupling finite element stiffness matrix and considered the frequency response functions from theory and experiments. Janusz [8] analysed the character of the rotor's longitudinal vibration with large misalignment. Guan et al. [9] proposed two kinds of dynamic models of shaft misalignment.

Simulation and experiments have been done. Michael et al. [10] compared the spectral analysis, orbitals, and the entire spectrum. It is found that full spectra can distinguish imbalance from misalignment by looking at forward and reversed phenomena. Sekhar et al. [11] used higher-order finite elements to develop reaction forces and moments due to flexible coupling misalignment. Wan et al. [12] used a numerical integration method to analyse a multi-disk rotor's non-linear dynamic behaviours and stability supported by an oil-lubricated journal bearing with coupling misalignment. Li et al. [13] used simulations and experiments to research a multirotor bearing system's dynamic behaviours and vibration mechanisms with parallel and angular misalignments. Feng et al. [14] studied the bearing misalignment of an inner-and-outer dual-rotor system of an aero-engine with numerical calculation. Li et al. [15] established a dynamic model of the misalignment fault of a twin-spool rotor with inter-shaft bearing. The vibration features of high- and low-pressure rotors were revealed by numerical analysis and experiment.

Other specialists [16-20] dealt with the causes of bearing misalignment and shaft deflection in rotary machines, as well as the generation of numerical models, while the consequences of operating in unsuitable conditions were analysed by researchers [21-27]. To eliminate this phenomenon has been enabled by increasingly precise production technologies, advances in new materials and other new inventions over the last few years, which have made it possible to use so-called self-equalising bearings. The most substantial and the most loaded part of such a bearing is a set of levers in which a pair of adjacent levers is always in contact. There are several types of levers (within various types of bearings) in the market; however, the development in this field continues, and companies try to find the best reliable solutions to ensure their competitiveness.

The presented research deals with some basic steps involving comprehensive research related to the development of a new self-equalising thrust bearing, and it focuses on the design of a system of its most crucial part, the so-called lever, that is responsible for the proper equalising functionality of such a bearing. The goal of the study has been to design a new type of lever geometry, to create its numerical model, and by means of numerical analysis and calculations to predict its useability in real conditions, that was verified by experimental tests of the lever itself as well as the bearing in operating conditions. The lever was modelled in two sizes, which suit the bearings representing the most often used types in powerful machines. The novelty of the research lies in the design of the newly developed geometry of the lever itself in order to create a basis for the design and production of a new self-equalising thrust bearing, in which the stress calculation according to von Mises hypothesis was applied, as well as contacts and stiffness according to Hertz's theory.

2. Self-equalising trust bearing characteristics

In order for a bearing to perform its function optimally, it must first be calculated correctly - that is, it must have the correct geometric dimensions. Another condition for an optimally working sliding bearing is a suitable choice of materials. The biggest problem is often the incorrect machining of the geometrical (micro-geometrical) shape of the functional surfaces. If the machining technology or strategy is incorrectly selected, the surfaces can, for example, be corrugated and thus do not meet the theoretical assumptions of an ideal surface or an ideally designed shape. The deformation of functional surfaces can also occur due to the thermal loading of components. An important role also plays the roughness of the functional surfaces of the sliding bearing. Improper roughness can cause rapid wear, damage, or destruction of functional surfaces due to insufficient lubrication [28].

The amount of permissible deviation from the parallelism of the bearing axis with the shaft axis also depends on the circumferential speed and the magnitude of the load. If the deviation is greater than the permissible, steps must be taken to adjust the overall solution or use a special bearing to compensate for this deviation [29].
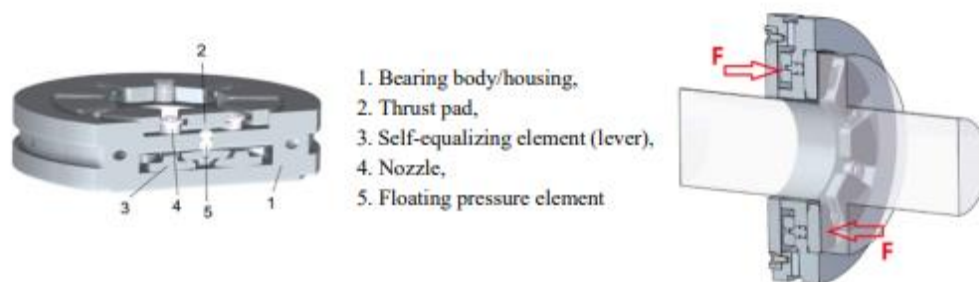
Fig. 1. Essential bearing components of a self-equalising thrust bearing and a load transmission by means of the levers [30].

Currently, the only solution that can capture the misalignment of the bearing axis with the shaft axis is a system of levers within the so-called self-equalising bearing **(Fig. 1) [30]**. The levers' system must be designed and manufactured so that it can transfer the pressure/force acting on the lower part of the bearing to the upper part of the bearing so that the axial segments of the bearing are always in contact with the shaft collar.

At least two elements are required for the slide bearing - the bearing itself and the rotor collar. The sliding bearing contains segments to which lubricating oil is supplied. Each segment is a separate carrier part of the bearing. The bearing surfaces (both bearings and shaft collars) are completely separated by an oil film with approximately a thickness of 20-40 μm due to hydrodynamic lubrication. The oil film avoids the risk of contact and, therefore, abrasion of the bearing surfaces **[31].**

It is the reason why in the case of the thrust bearing, the most critical part is a system of very precise manufactured levers, which are in close contact each to other, so they must be not only correctly designed from the geometrical point of view, but the critical role also plays a quality of the functional surfaces of these levers. The set of levers aims to distribute the load evenly over the entire circumference of the bearing that is transferred to the bearing housing and subsequently to the machine frame, even in the case of undesirable misalignment of the shaft and bearing axes.

The bearings used in compressors usually include 6-10 segments because of the large difference between the small and large diameters of the collar's annulus of the active surface. Conversely, turbines can use up to 18 (or more) segmented thrust bearings **[32].**

The levers form a closed chain, which is best solved by the absolute (complete) interchangeability method. This approach allows the assembly of all components that make up the individual chain links, made to the prescribed dimensions and relatively narrow tolerances (determined by solving the dimension chains by maximum and minimum methods), without prior selection, adjustment, or fitting, and ensures full accuracy of dimensional closing members.

For every thrust, the pad is necessary to use two levers. For example, it means that it is necessary to use 36 levers at 18-pads bearing.

Ideally, the forces acting on the levers should be the same at every lever (**Fig. 2**), but due to passive resistances, inappropriate geometry of the levers, and also the rolling of the levers themselves when the arms change forces and thus moments, these forces have declining character, as it is shown in **Fig. 3.**

It is evident that there are many contacts with a relatively small area. At contact in real practice, it is not the geometric area that matters, but the actual contact area, which is smaller and only exceptionally equals the geometric area. In the ideal case of two perfectly smooth elastic bodies, the classical Hertz relations are applied **[33].**

For the faultless function of the so-called self-alignment, it is necessary for the upper and lower levers to roll with each other. However, this cannot be wholly ensured, and therefore the reality is probably such that the levers perform a general movement relative to each other, rolling with friction. This movement must be smooth even after millions of cycles. It means increased demands on the contact area between the levers. Since such a bearing is intended mainly for steam turbines or turbochargers, there will be several forms (combinations) of load:

- Static load. The specific value of the static load is usually known from the manufacturer of the equipment (turbines, turbochargers), and it is very easy to calculate (but also experimentally verify) whether the lever (or the surface of the lever) can withstand this static load.
- Dynamic load. This load can be further divided into two subgroups:
  - Frequency - this load is strongly dependent on the dominant frequency of the turbine/turbocharger (in the case of using a bearing in a turbine, this value is 50 Hz in Europe and 60 Hz in the USA. This dominant frequency component is reflected in

vibrations within tens of microns and result in micro-friction between the levers and subsequent so-called "fretting".

- Random (independent of the dominant frequency of 50 or 60 Hz) - this load depends primarily on the dynamic characteristics of the machine design and namely its rotor, on the thermal deformation of the whole set, on the overall deflection of the shaft, but also inaccuracies in production. This variable load is manifested in the contact between the levers in that the levers roll or slip within millimetres.

Of course, everything (every load) happens at once (static load + micro-friction + friction + rolling).

Based on the above, it is clear that the requirements for the material of levers have to be high. It has to possess good mechanical and tribological properties, taking into account surface integrity aspects. Several materials could be used for this purpose, but one of the most commonly used in the production of bearings and meets the required characteristics of a highly stressed functional component is DIN 34CrNiMo6 steel. It has high strength, high toughness, and good hardenability [34].
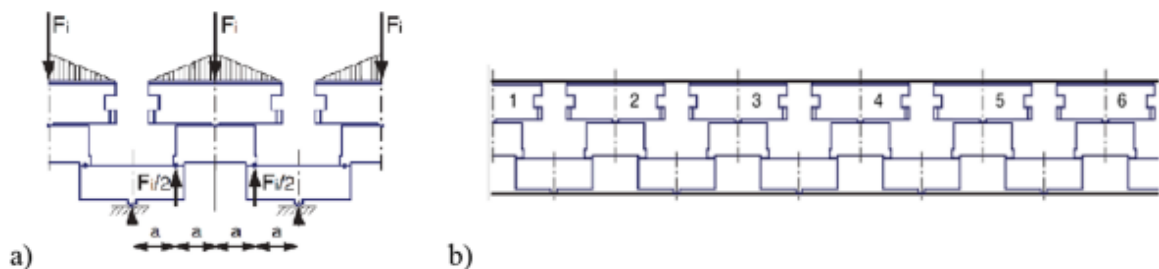
Fig. 2. a) Ideal force distribution at the levers; b) lever tilting without the shaft deflection (misalignment).
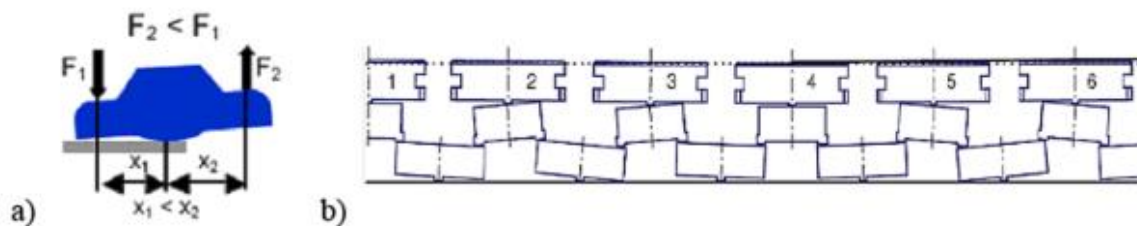
Fig. 3. a) Real force distribution at the levers b) principle of the lever tilting at the shaft misalignment.

The chemical composition of the 34CrNiMo6 steel is in **Table 1**.

Based on the long experience of the bearing manufacturers with this material, 34CrNiMo6 steel was also selected as the material for the production of a bearing prototype. It is heat-treated, low-alloy steel with high hardenability and strength, containing nickel, chromium and molybdenum. In addition, the 34CrNiMo6 steel has very good toughness properties with a Charpy V-notch at a low temperature. In the actual production process, the typical heat treatment of this steel includes two stages, quenching and tempering. The 34CrNiMo6 steel can achieve high strength after quenching to a fully martensitic structure, while the ductility and toughness can be improved by tempering [34].

3. Development and analyses of a lever system for a newly designed self-equalising thrust bearing

3.1. Preliminary design of a new lever geometry

A simple experimental test was proposed to perform to specify which geometries and shapes is the most suitable in terms of the kinematic functionality of a bearing, see **Fig. 4.** A comparative experiment was carried out in collaboration with GTW Bearings to determine whether the assembly works appropriately, what is its maximum deflection and whether it is worthwhile to deal with the tested geometry.

The measured bearing was divided into four quadrants (see **Fig. 4b**). Each quadrant was gradually loaded. The maximum bearing deflection was then monitored in the quadrant that was loaded and then in the quadrant that was opposite this loaded quadrant. The principle of measuring the maximum deflection was, therefore, to continuously load the bearing through the ground plate using a clamp on one side (e.g., quadrant "A") and to continuously lightening the bearing through the ground plate using a clamp on the other side (in this case it would then was quadrant "C".). The deviation value was read on the dial indicators.

At the research beginning, three basic variants of lever geometry were designed, and their prototypes were produced. Their sizes corresponded to a bearing with 18 segments on a pitch circle of 516 mm that was chosen as a reference bearing for measurements. It represents (with its size and number of segments) the top level of self-equalising bearings intended for industrial turbines.

The first initial design (**Fig. 5**) of the levers was conceived, so the contacts between both arms of levers were of the type of "radius -plane" with a large bottom radius due to rolling movement. The values measured during the experimental test are listed in **Table 2**.

It is clear from the measured values that the lever system did not work properly. Deflection values 0.07 ÷ 0.2 mm mean a deflection angle of 0.024° ÷ 0.031°. It is one level lower of angle deflection than required.

Due to the significant differences between the deflections in the quadrants, it is evident that there were considerable elastic deformations, which together with the large lower radius for rolling movement generated such losses that no loading force would transfer to the opposite quadrant.

The *second version* of a lever design (**Fig. 6**) was developed based on feedback from the measurements of the 1st version, and it tried to suppress its weaknesses. The stiffness was multiplied, and the lower rolling radius was decreased by an order of magnitude. Furthermore, "cut-outs" and protrusions were made on the levers, which served as stops of the levers in the extreme (limit) positions and also for the smooth flow of oil, which the initial design did not sufficiently take into account.

The contact between the levers was conceived here as " Cylinder to Cylinder" + "Plane to Plane" with a small lower radius for rolling movement. This set-up aimed to reduce the sensitivity of the lever system to manufacturing tolerances along with the higher functionality of the entire system.

As a result of these modifications, the kinematics of the mechanism has significantly improved, and the result can be seen in **Table 3**.

Table 1 Chemical composition of the 34CrNiMo6 steel [34].

Component	C	Mn	Si	P	S	Cr	Ni	Mo	V	Cu	Al
(%)	0.34	0.793	0.282	0.0196	0.0052	1.72	1.55	0.221	0.0092	0.193	0.0194

a)   b)

Fig. 4. Basic assembly of measuring equipment, b) division of the bearing into 4 quadrants.
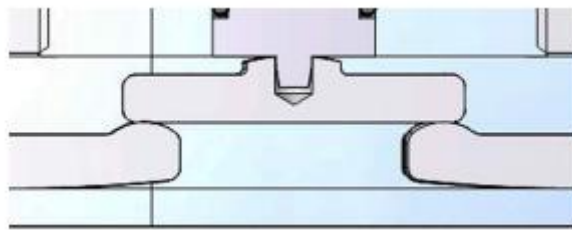
Fig. 5. The 1st (initial) design of the lever geometry.

Table 2 Measured values of angle deflection for the 1st (initial) design of the lever geometry.

Loaded quadrant	Quadrant of deflection				Angle of deflection (°)
	A (mm)	B (mm)	C (mm)	D (mm)	
A	0.18	–	0.1	–	0.031
B	–	0.15	–	0.07	0.024
C	0.07	–	0.18	–	0.028
D	–	0.08	–	0.2	0.031
Average					0.029
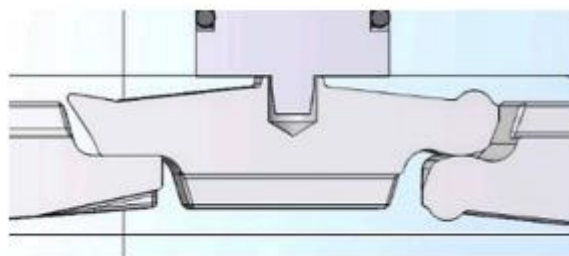
Fig. 6. The 2nd variant with contact couples "Cylinder/Cylinder "+ "Plane/Plane ".

Table 3 Measured values of angle deflection for the 2nd design of the lever geometry.

Loaded quadrant	Quadrant of deflection				Angle of deflection (°)
	A (mm)	B (mm)	C (mm)	D (mm)	
A	0.25	–	0.3	–	0.061
B	–	0.2	–	0.25	0.050
C	0.3	–	0.25	–	0.061
D	–	0.25	–	0.3	0.061
Average					0.058

It is clear from the measured values that the lever system was already working almost correctly. Deflection values of 0.2 ÷ 0.3 mm mean a deflection angle of 0.05° ÷ 0.061°, which is already an angle closer to the required input of 0.1°.

The differences between the deflections in individual quadrants are negligible in this case, and it can, therefore, be argued that such elastic deformations no longer occurred and that the losses, generated by this mechanism in the form of elastic deformation and friction, could already be overcome by the loading force exerted by the bolted joint.

Given that the stiffness was already found to be sufficient, *the third design* (shown in **Fig. 7**) was focused on the microgeometry of the levers in order to further improve the overall kinematics of the levers. Furthermore, the "cut-outs" on the levers arms were modified to eliminate technologically unsuitable protrusions, which served as lever arm stops in the extreme (limit) positions and also for trouble-free oil flow. Due to the goal of finding the optimal geometry of the levers, they have been manufactured for assembly with the contacts of types "Cylinder/Cylinder" + "Cylinder/Plane".

As a result of these modifications, the kinematics of the mechanism was further improved, and the result can be seen in **Table 4**.

The stiffness and functionality of the designed levers in real working conditions were experimentally verified.

Fig. 8 shows a real produced lever and the setting of the lever during the static compression test. The lever was supported on both sides on hardened cylinders of the tested machine. Since the lever had a cylindrical contact area on one side and a plane contact area on the other side (**Fig. 8a**), both contact pairs (Cylinder/Plane and Cylinder/Cylinder) could be statically tested at the same time (**Fig. 8b**).

Because of the safety, the levers were tested only for a maximum load of 200 kN (**Fig. 9**). The large type of levers returned to their original shape after the load was completed (that was verified on a granite plate), which means the deformation of all levers took place in the area of elastic deformations.

For the small type of levers, plastic deformation already occurred at about 150-160 kN (**Fig. 9**), then the test was interrupted because the levers slipped out of the jaws (a vertical line down in the graph in **Fig. 9**). Small levers were not as rigid as larger variants, but if it considered that the nominal load on the whole bearing, where the small variant of levers is used, is a maximum of ~130 kN, which means that less than 11 kN comes out on one lever, it could then be stated that the safety static factor is thus more than 10.

After loading, the condition of the surface of each lever was checked for the occurrence of microcracks due to the effect of the load, which would initiate damage to the entire lever.

Although small defects were found in most of the levers, subsequent analysis using a scanning electron microscope showed that the integrity of the surface was not disturbed in the observed defects. Only impurities that appeared as defects when visually observed were present on the surface of the levers. In some cases, these were surface defects, the cause of which was the surface treatment technology of applying nickel coating **[35].**

Figs. 10 and 11 show the defects found on the nickel-plated surface of lever no. 31.

Based on the scanning electron microscope picture on the right side of **Fig. 10**, it could be stated that they are not related to static loading, but their origin is in the inhomogeneity of the surface. In another area of the same lever **(Fig. 11)**, a visual test, as well as scanning electron-microscopy, revealed defects related to the technology of the previous surface treatment, not to the static load. Thus, no defects or cracks caused by static loading were found on any of the levers.

Although, based on the obtained results, as the best variant from the measured deviation was the 3rd one, however, the design with contact pair Cylinder/Plane on both sides of the lever was selected for numerical analysis, that was the most suitable not only from the geometry point of view but also due to the fact that cylinder-to-cylinder contact is unsuitable in terms of stress (there is a very small area, where the extreme pressures and surface damage occur. The choice of this Cylinder/Plane contact pair configuration is also advantageous from the point of view of production because at both ends of the lever there is then a Plane/Cylinder contact, i. e. all levers are the same, only every second one is placed in an overturned way.

Before the FEM (Finite Elements Method) analysis, the ideal kinematic model was defined as the 3D model of a bearing with 18 segments (36 levers) with cycloid-controlled joints at rolling without friction without preliminary research that is presented in **Fig. 12**. An actual model includes the general joins (rolling with friction) between levers, although the goal is to minimise passive resistance caused by friction. The presented ideal kinematic model considers the rolling joins without friction. Such a system is statically determined, and the path of movement of individual points on the lever can be monitored employing cycloids, and the position of individual lever arms can thus be specified.

3.2. Numerical simulation of a new lever's geometry

The geometry with contact pair Cylinder/Plane on both sides of the lever (partially presented at the third design in **Fig. 7**), which resulted from preliminary experimental research, was subjected to further investigation.

The presented analyses were done for the bearings with external/internal diameters of segment pitch circle D_{small} = 345.4/231 mm or D_{large} = 549/336 mm using the Ansys software. They will be referred to as small and large bearing in this study. The dimensions of
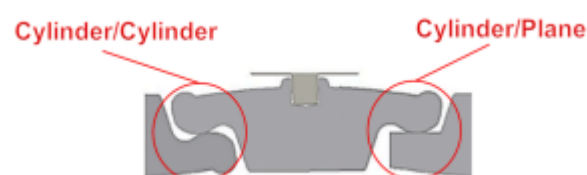
Fig. 7. The 3rd variant with contact couples "Cylinder/ Cylinder "+" Cylinder /Plane ".

Table 4 Measured values of angle deflection for the 3rd design of the lever geometry.

Loaded quadrant	Quadrant of deflection				Angle of deflection (°)
	A (mm)	B (mm)	C (mm)	D (mm)	
A	0.3	–	0.35	–	0.072
B	–	0.4	–	0.3	0.078
C	0.35	–	0.4	–	0.083
D	–	0.4	–	0.35	0.083
Average					0.079

a) b)
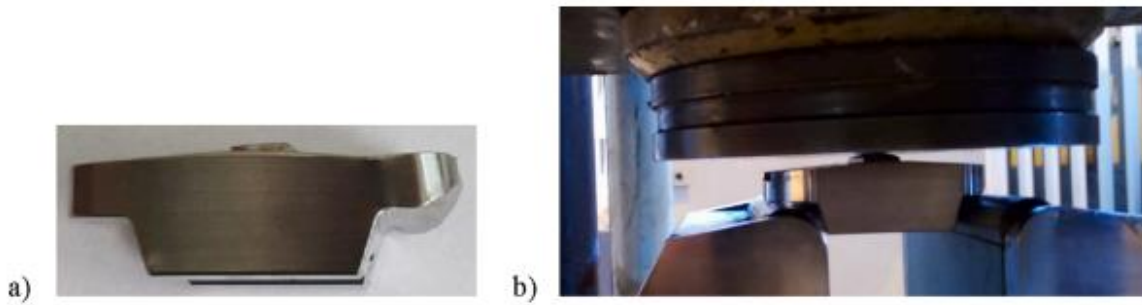
Fig. 8. Produced lever and its positioning within the test equipment during the static compression test.
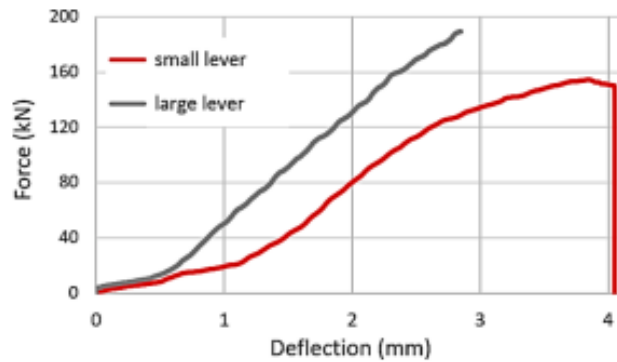
Fig. 9. Dependency of loading force and deflection.
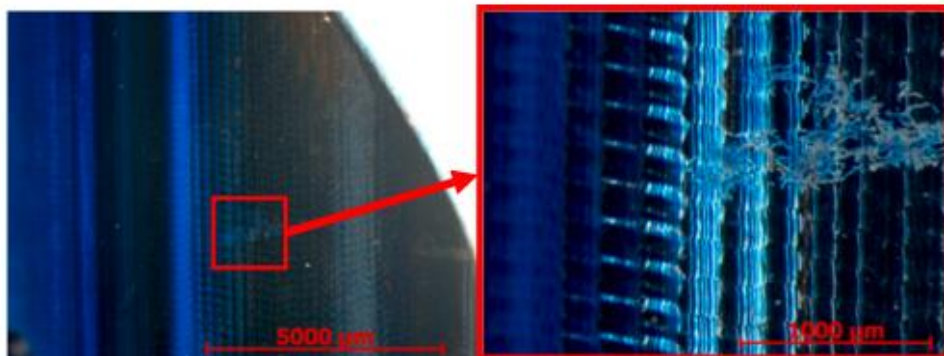
Fig. 11. The lever no. 31 - defects related to the surface treatment
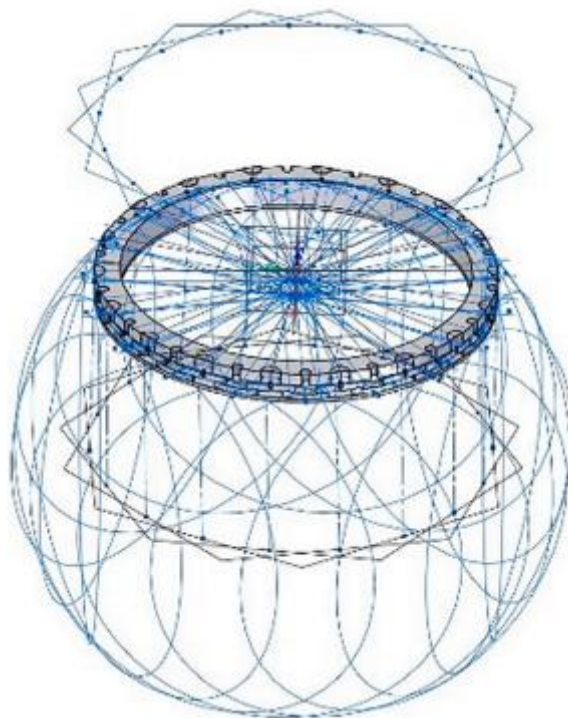
Fig. 12. Kinematic model of lever paths for the final version of bearing with 18 segments (36 levers).

The dimensions of the levers affecting the stress concentrator have been considered according to **Fig. 13**, and they are for small/large bearing as follows: l = 4.4343/5.2804 mm; b = 29.0017/53.0239 mm and h = 6.533/11.272 mm. The dimensions were used to compile the program for fast interpolation calculation of the stress concentrator according to known FEM results of 3 lever sizes.

To have a start point idea about the behaviour of a new self-equalising bearing, the numerical analyses of the levers/bearing were carried out in cooperation with New Technologies Research Centre at West Bohemia University in Pilsen in the Czech Republic.

The axial bearing self-balancing system model is cyclically symmetric, as shown in **Fig. 14**a. Minor asymmetries caused by the dividing plane of the bearing do not affect the balancing function and could be neglected in the model. Thus, two whole levers can be included in one symmetrical segment. A

solution was chosen where the symmetrical segment contains the entire lower lever arm and two halves of the upper lever arm, as shown in **Fig. 14b [36].**

The boundary conditions were applied so to prevent the movement (collapse) of the system and at the same time use them to influence the stress distribution in the levers as little as possible. Therefore, circumferential movement (in the direction of the bearing circumference) was forbidden in the entire section plane of the upper lever. For numerical stability of the calculation, one point of the upper lever in the radial direction, two points on the lower lever in the radial direction and one in the circumferential direction were also limited. These conditions prevented radial displacements of the entire levers and their rotation around the "z" axis (axial direction).
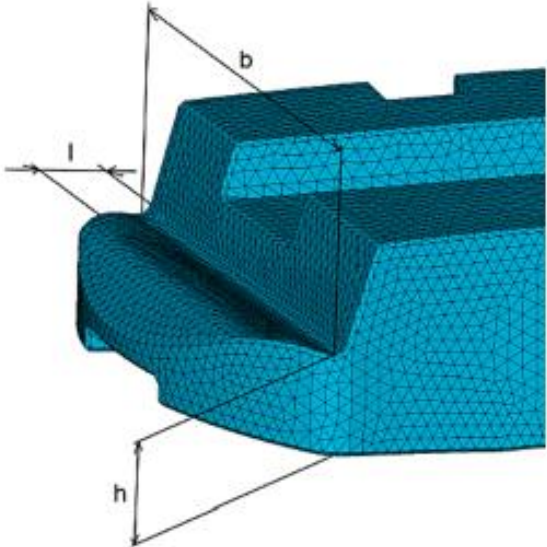
Fig. 13. Important sizes of a lever.
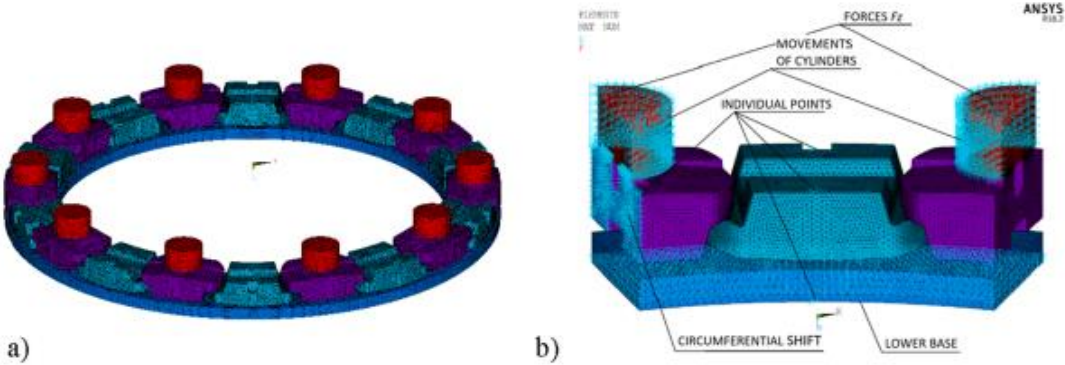
Fig. 14. a) Cyclically symmetric model of the whole balancing system, b) the numerical model **[36].**

Contacts in Ansys were modelled by elements Conta174 and Targe170. The contacts are without shear friction. Finding the right combinations of contact parameters for a converging solution was not easy because the contacts are in series, and both the upper and lower lever arms are loaded only through these contacts. The Ansys manual also points out that this situation can be numerically problematic [37]. If contact were to be studied, only a model of its immediate surroundings with much more fine discretization would need to be made separately. Due to this, although finally, the settings of contacts have been able properly to transfer the load between individual segments, it has been not possible to consider the values of stress in a close area of contact to be reliable, so the analytical computation according to the Hertz theory was used for that.

The numerical model has been defined of the non-linear type considering big deformations with contact elements defined in joints. A load of bearing was set up based on the real values provided by GTW company (Czech Republic) that was measured in real practice at one of the industrial stream turbines and from which results that small bearing can be standardly loaded with an axial force of 128 kN and large bearing with the force of 393 kN. The load has been evenly distributed on all bearing segments within the analysis, although it can be slightly different in real practice.

Steel 34CrNiMo6 has been used for the analysis. The material of the numerical model is considered elastic with a modulus of elasticity E = 2.1e5 MPa and Poisson's ratio μ = 0.3. Finite elements were chosen of type Solid185. It is an eight-node 3D element for modelling solid structures. It supports many different load models, including large deformations. The nodes have 3 degrees of freedom (x, y and z offset). The shape of the element can be reduced in various ways by merging nodes. In these calculations, the shape of a tetrahedron is used, which best discretises even geometrically very complex shapes. FEM models of the small/large bearings have been created by 75.280/138.508 nodes and 369.446/673.242 finite elements, mostly four-wall elements. There are 2D triangle elements only in the contacts.

3.3. Contacts according to Hertz theory

As discussed above, in this case, the finite element method cannot reliably calculate the stresses and deformations around the contacts between the lever arms themself, between the lever arms and the pressure rollers, and between the lever arms and the bottom plate. Therefore, Hertz's elastic contact theory was used to calculate the stresses and deformations around the contacts.

The maximal Hertz pressure for Cylinder/Cylinder contact, when one of the cylinders is infinite radii (plane), is given by equation [38].

$$p_{Hmax} = \frac{2F}{\pi b l} = \frac{2F}{\pi \times \sqrt{\frac{2F}{\pi l} \times \frac{(1-v_1^2)/E_1 + (1-v_2^2)/E_2}{1/d_1 + 1/d_2}} \times l} \tag{1}$$

where F is a load of a lever; v_i is Poisson material constant; E_i is the modulus of elasticity; d_i is the diameter of a cylinder; l_i is the length of a cylinder, i is an order of a cylinder.

The loading force of the lever arm has been calculated based on the axial bearing force 128 kN for small bearing. Since the bearing includes 12 segments with the load distributed on two arms of lever, the axial force has been divided by 24. So, the total value of continuously distributed force on the lever

arm has been 5.333 kN. Similarly, it has been calculated at large bearing, at which the force 393 kN was divided by 20 since it includes 10 segments. In this case, the considered force was 19.65 kN.

Hertz's theory of elastic contact of bodies uses methods for solving the boundary value problem for elastic half-space. The dimensions of the contact surfaces must therefore be substantially smaller than the dimensions of the body as well as the radii of curvature of the contact surfaces. The first condition ensures that the stress field is not significantly affected by the proximity of the body boundaries (thus not depending on the shape of the bodies in contact), and the second condition ensures that the area around the contact can be considered as a planar half-space interface and that the stresses are small enough to remain within the scope of the linear theory of elasticity. Furthermore, it is assumed that only normal loads act between the surfaces in contact. Surfaces must therefore be considered with a zero coefficient of friction **[38]**.

Hertz's theory is therefore based on the following assumptions: **[39]**.

1. Solids have a continuous surface and are non-conforming (i.e., do not fit together).
2. The deformations are "small", i.e., the dimension of the contact surface is significantly smaller than its radius of curvature.
3. Each body is considered to be an elastic half-space, i.e., the dimension of the contact surface is substantially smaller than the radii of curvature of both surfaces and then the dimensions of the bodies.
4. Surfaces are without friction; acting forces (pressure) are only normal.

According to Hertz's theory, calculations of general contacts are usually performed in a simplified procedure using pre-calculated tabulated coefficients **[33]**. Here, however, a program for the accurate calculation of contacts according to Hertz's theory was created, including the solution of equations with elliptic integrals for the general contact of two elastic toroids. Here, the program was used to calculate deformations and stresses in the contact of elastic cylinders, or more precisely, its special case of Cylinder/Plane contact.

4. Results and discussions

4.1. Numerical analysis

At the analysis of the small bearing, it was found that the maximum value of the vertical displacement reached 0.053 mm. A small inclination of the levers towards the outer circumference of the bearing is also observable here **(Fig. 15**

The maxima of the dominant vertical stress in the inner corners of the lever arms reach the values σ_z = 134 MPa in tension. Only the pressure values σ_z in a close area of the lever arm contacts are higher. According to the HMH (Huber - von Mises - Hencky) hypothesis, the reduced stress reaches a maximum value of approximately σ_{HMH} = 180 MPa in the corners of the lever arms. Again, only the values in the local area of the lever arm contacts are higher.
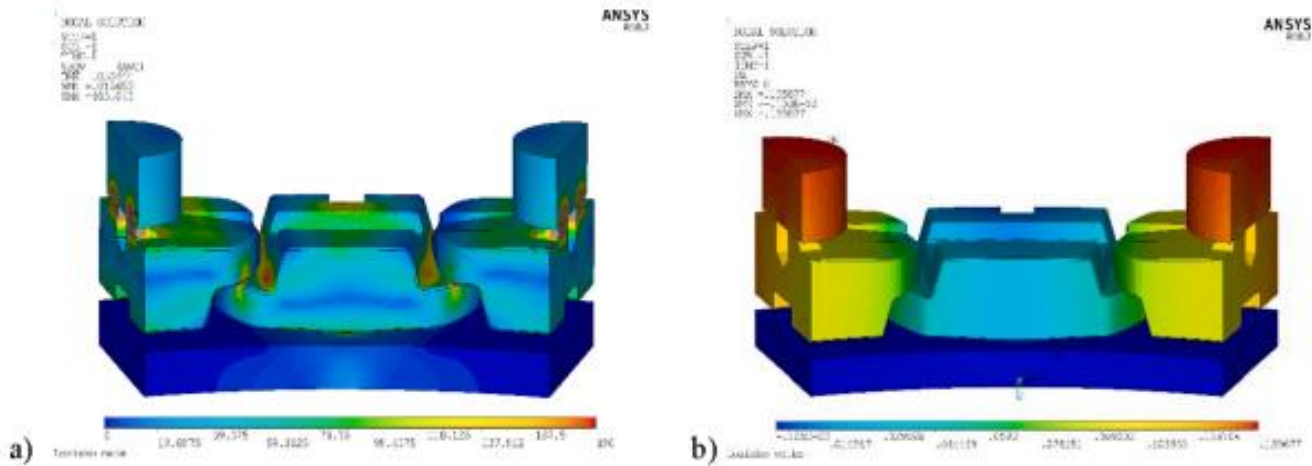
Fig. 15. The examples of reduced stress distribution (ohmh) (small bearing), b) Distribution of vertical displacements on the balancing system (large bearing).

On the upper surface of the lower lever arm between the groove for the pin limiting the radial movement of the lever arm and the longitudinal oil groove on the lever arm, the stress is approx. σ_{HMH} = 130 MPa mainly due to the tensile stress in the "x" direction. At the edge of the groove for the pin, it is locally approximately σ_{HMH} = 190 MPa.

The distribution of vertical displacement, vertical stress and reduced stress are similar at large bearing; only the values differ. As expected, the maximum values of the vertical feed are on the faces of the pressure rollers, namely approx. 0.14 mm. There is a slight inclination of both levers towards the outer circumference of the bearing. The predominant stress is the stress in the vertical direction (σ_z). In addition to the close vicinity of the contacts, its maximum values are tensile, up to about 224 MPa in the inner corners of the lever arm.

The reduced stress, according to the HMH hypothesis (σ_{HMH}), has maxima again in the vicinity of the contacts and further in the mentioned corners of the lever arms, namely about 270 MPa. Another increased value of σ_{HMH}, approx. 150 MPa, lies on the upper surface of the lower lever in the area between the recess for the pin securing the circumferential movement of the lower lever and the longitudinal oil groove on the lever. The higher value of σ_{HMH} is given here mainly by the tensile component σ_x. At the edge of the pin, the σ_{HMH} value of approx. 240 MPa is locally achieved by the notch effect of the edge. Because the selected 34CrNiMo6 steel that has been used for the levers in a refined state has a yield strength of 900 MPa, the stress values of the levers can be considered safe.

Reduced stress distributions (σ_{HMH}) on the root of levers are shown in Fig. 16.

It can be seen from Fig. 16 that the stress along the width b of the lever is not evenly distributed. There are several reasons for this, in particular:

- the longitudinal groove on the back of the lever arm for oil flow causes a decrease in stiffness in the middle of the lever arm width, σ_{HMH} is reduced in the middle,
- the length of the force arm increases towards the outer circumference of the bearing, thus changing the loading bending moment,
- the kinematics of the movement of the levers causes a not exactly definite contact along its length.

As the numerical value of σ_{HMH}, the maximum value occurring anywhere along the width b of the lever arm was chosen; it was 185.8 MPa for small bearing and 249.3 MPa for large bearing.

4.2. Contacts and stiffness according to Hertz theory

All the contacts in the self-balancing thrust bearing system could be described as a 1D contact of the Cylinder/Plane pair. When calculating, the reference points in both bodies at a sufficient distance from the contact points (with respect to the width of the contact area) were selected. Among them, the deformation, according to Hertz's theory, was calculated.

Three contacts were considered within the analysis.

- the first is the case of contact of the upper lever with the pressure cylinder (hereinafter referred to as "Contact 1");
- the second case with a smaller radius of curvature of the contact surface and also with a smaller (half) transmitted force is both contacts between the levers to each other (hereinafter referred to as "contact 2");
- and the third is the case of contact of the lower lever with the lower sheet plate (hereinafter referred to as "Contact 3"). It differs from Contact 1 in its length because it is not interrupted by the hole for the locking pin.

Then the vertical displacements from these reference points were subtracted from the relevant FEM calculations, and their difference was replaced by the result according to Hertz. By calculating the contacts according to Hertz's theory, more reliable values of the total deformation of the force chain of the self-equalising system were obtained, which are given in **Tables 5 and 6**.

It is visible from the Tables that the deformations calculated according to Hertz's theory are several times larger than the results of the FEM calculation.

In spite of that, regarding the magnitude of the maxima of the compressive contact stress, the values can be considered safe, even though these maxima reach values of up to 2.5 times the yield strength (for the used material 34CrNiMo6 in the tempered state σ_{yield} = 900 MPa). The maximum compressive stress is in the middle of the contact surface, where spatial stress - all-around pressure occurs. The steel can thus safely withstand pressures of 3,500 to 4,000 MPa, as it is referred to in **[40,41]**.

To assess the strength of the material, it would be necessary to start from the main stresses and use one of the strength theories. The critical stress point even does not lie at the maximum contact pressure point but a certain depth below the surface **[42]**.

It has been shown that the design of the tilting segments in the bearing housing significantly affects the properties of the entire segment bearing. In the case of bearings without suspension or a self-aligning system, this is primarily the contact rigidity of the supports of the segments supported on the bearing housing.

In the case of self-aligning bearings, the rigidity of the segment mounting is then even more significantly affected by the design of the entire balancing system. Its stiffness affects the overall stiffness of the bearing assembly (and thus the stiffness of the shaft bearing), which is one of the determining parameters of the dynamic behaviour of the entire rotor system **[43,44]**.
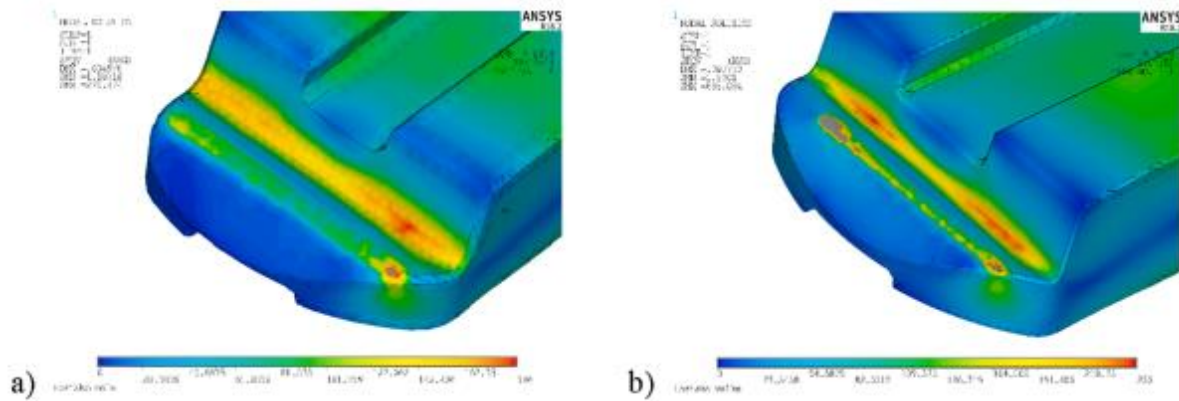
Fig. 16. Reduced stress distribution (cHmH) on the root of levers a) small bearing (left), b) large bearing.

Table 5 Results of the calculation of the maximum compressive stress and deformations between the selected reference points for a small bearing.

Contact type	Radius of curvature (mm)	Contact length (mm)	Transmitted force (N)	Deformation (mm)		Maximal stress (MPa)
				FEM	Hertz	Hertz
Contact 1	10	10.147	10.667	0.00616	0.01711	1.965
Contact 2	6	22.593	5.333	0.001851	0.00494	1.202
Contact 3	10	16.160	10.667	0.004808	0.01336	1.557

Table 6 Results of the calculation of the maximum compressive stress and deformations between the selected reference points for a large bearing

Contact type	Radius of curvature (mm)	Contact length (mm)	Transmitted force (N)	Deformation (mm)		Maximal stress (MPa)
				FEM	Hertz	Hertz
Contact 1	16.5	20.652	39.300	0.01906	0.0316	2.059
Contact 2	10	33.819	19.650	0.002151	0.01173	1.461
Contact 3	16.5	31.16	39.300	0.011445	0.02391	1.676

To calculate the stiffness, the balancing system's whole force and deformation chain were considered (see **Fig. 17**). In this case, this begins with the pressure roller's upper surface, including roller deformation, roller-to-upper lever contact, upper lever deformation, lever contact deformation, lower lever arm deformation, and lower lever-to-bottom plate contact, including sheet metal deformation. Contact between the pressure roller and the sliding segment, as well as deformations of the sliding segment itself, was not included in the stiffness calculation.

As it was already said above, in the areas of all three contacts, the deformations between the reference points calculated by the FEM were replaced by more reliable values of deformations calculated according to Hertz, see results above. Other deformations (i.e., deformations of the bodies themselves) remain calculated using FEM. The results are shown in **Table 7**.

The comparisons of the oil film stiffness and the contact stiffness of the tilting segments of the particular radial bearings produced have shown that the contact stiffness is only approximately 2 to 5 times higher than the oil film stiffness. It is thus clear that the rigidity of the whole balancing system,

even with three contacts in series, cannot be neglected due to the rigidity of the oil film in the correct calculations.
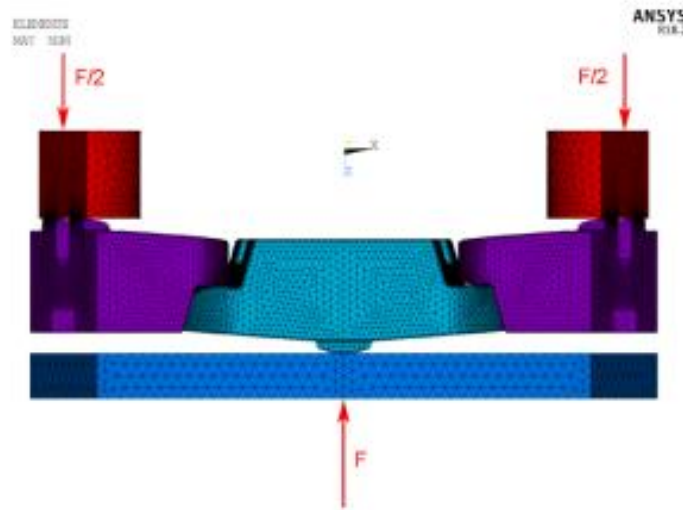
Fig. 17. Numerical model for stiffness calculation.

5. Experimental verification of the lever design

The experimental static test described within **Section 3.1** was of a short-term nature. From the point of view of testing the durability of the levers, primarily on fatigue, it did not have a sufficient corresponding value. This was subsequently confirmed after disassembling the levers from individual prototypes when the levers showed zero wear.

To comprehensively verify the design of the bearing, it was necessary to test the bearing in an experimental device that can simulate real operation. However, these experiments did not aim to verify the durability of the levers but to verify the overall functionality of the newly developed type of bearing. Levers using a Cylinder/Plane contact pair on both sides were used for reliability and operability validation of bearing prototypes. The functional surfaces of the levers were machined to Ra = 1 µm based on the research **[35]**. The levers were subsequently surface strengthened by electroless nickel plating.

The TG 10 experimental turbine located in the DOOSAN Skoda Power research centre is a device on which the geometry of the turbine blades is primarily tested. It is a single-stage turbine capable of rotating at more than 10,000 rpm speeds. In order for the turbine to be under a specific load, it is braked by a hydraulic brake representing the generator. On the one hand, the turbine is equipped with a combined plain bearing and, on the other hand, a radial bearing with tilting segments. The turbine set in this way is able to simulate real load conditions that act on the bearing during operation. For this reason, this device was selected for comprehensive verification of the self-equalising bearing functionality.

For testing in the experimental TG10 turbine was used 8-segment axial bearing with levers on a pitch circle 336 mm (**Fig. 18**), which was inserted into the body of the combined bearing on both sides so that it was possible to capture the axial component of force from both sides (so-called active and

inactive sides turbines). This prototype design completely fulfilled the requirement of modularity of the combined bearing solution.

Measured temperatures and force loads of levers in the newly developed axial thrust bearing on the active side are in **Fig. 19**.

It can be seen from the graph that the self-equalising mechanism in the bearing worked very well even at full load because the measured temperatures in the lower and upper segments were almost identical. In absolute terms, the temperatures of both segments were well below the possible maximum, which is around 115° C.

The bearing was also equipped with sensors for measuring the magnitude of the axial force, so it was possible to measure the functionality of the mechanism from the point of view of the distribution of forces acting on the upper and lower segments. Even in this case, the difference was insignificant.

6. Conclusions

The main cause of bearing damage is misalignment between the shaft and bearing axis. One of the ways to increase the reliability of bearings and reduce the risk of their sudden failure, besides monitoring them, is to use so-called self-balancing bearings. In the case of the thrust bearing, the most critical part is a system of very precisely manufactured levers that are in close contact with each other. Therefore, they must not only be correctly designed from a geometrical point of view, but the quality of the functional surfaces of these levers also plays an important role.

Within the presented research, a new lever (lever system) of the self-equalizing thrust bearing has been designed using the kinematic and numerical analyses, results and stiffness of the lever were confirmed by static compression test, and the functionality of the complex new developed bearing was verified by its implementing in real operating conditions employing DOOSAN Eikoda Power TG 1.

- As part of the preliminary research, three types of lever geometry were proposed. The levers and bearings were produced and experimentally tested for bearing deflection angle in order to select which one would be worthy of further investigation.
- The best variant from the view of geometry and the measured deviation was the 3rd one with the contact pairs Cylinder/Cylinder and Cylinder/Plane, so this type of the lever design was selected for numerical analysis, at which the behaviour of levers with two sizes was investigated under a static load.
- A numerical model was established, and two bearings with different sizes were analyzed. Reduced stresses according to the HMH hypothesis (aHMH) and the analytical computation according to the Hertz theory confirmed that the levers are stiff enough and that the selected material (steel 34CrNiMo6) can withstand several times higher load than occurs in real operation of equipment.
- Experimental static tests confirmed the stiffness of the levers, while no defects or cracks caused by static loading were found on any of the levers. Although the levers proved to be sufficiently rigid and could withstand both load and imprint in the press, the authors were aware that fatigue could be a problem with dynamic loading even with an otherwise sufficiently statically dimensioned structure.
- To verify the overall functionality of the bearing, the TG 10 experimental turbine located in the DOOSAN Skoda Power research centre was used. Measured

temperatures and force loads of levers in the newly developed axial thrust bearing were measured, and the results proved that the bearings can safely and reliably work in real operating conditions.

Table 7 Results of calculations of stiffness of self-equalising system of the analysed bearings using deformation of contacts according to Hertz's theory.

Bearing type	Transmitted force (kN)	Total deformation (mm)		Stiffness (kN/mm)
		FEM	Hertz	
small	10.667	0.05294	0.0755335	141.222
large	39.300	0.13416	0.1687441	232.897
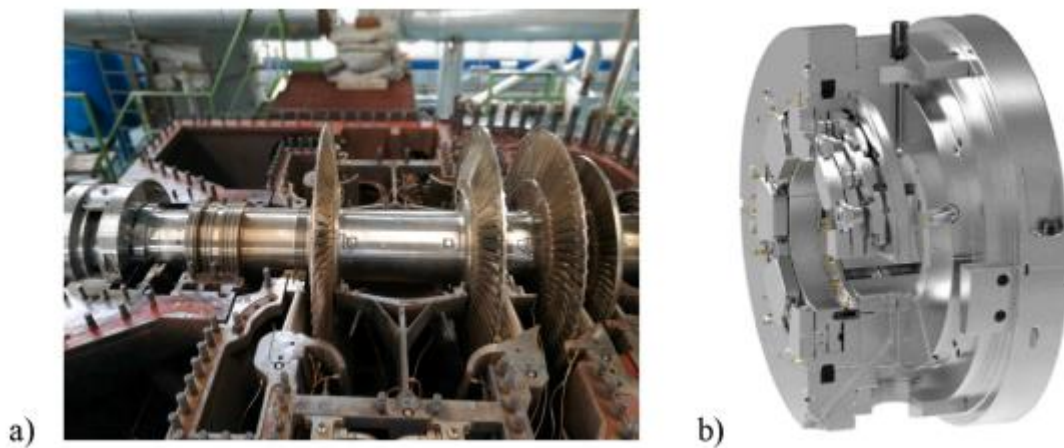
Fig. 18. DOOSAN Skoda Power TG 10 experimental turbine, a) assembly, b) detail of combined plain bearing (section).
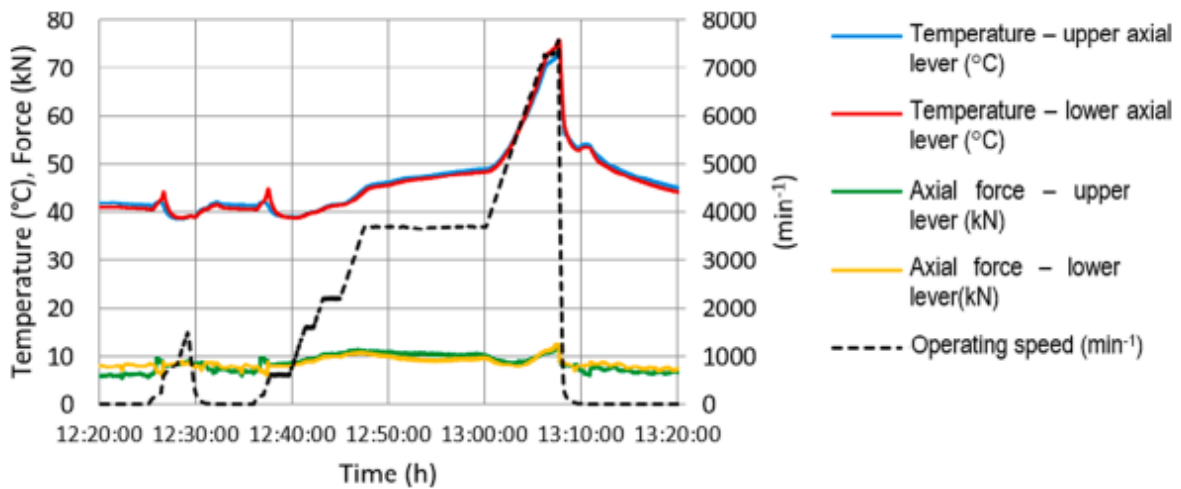
Fig. 19. Measured temperatures and loads of thrust bearing segments (active side) in time.

References

[1] T.H. Patel, A.K. Darpe, Vibration response of misaligned rotors, J. Sound Vib. 325 (3) (2009) 609-628.

[2] A.K. Verma, S. Sarangi, M.H. Kolekar, Experimental investigation of misalignment effects on rotor shaft vibration and on statorcurrent signature, J. Fail. Anal. Prev. 14 (2) (2014) 125-138.

[3] V. Hariharan, P.S.S. Srinivasan, Vibration analysis of misaligned shaft-ball bearing system, Indian J. Sci. Technol. 2 (2009) 45-50.

[4] A.M. Umbrajkaar, A. Krishnamoorthy, Modeling and vibration analysis of shaft misalignment, Int. J. Pure Appl. Math. 114 (2017) 313-323.

[5] N.F. Wang, D.X. Jiang, Vibration response characteristics of a dual-rotor with unbalance-misalignment coupling faults: theoretical analysis and experimental study, Mech. Mach. Theory 125 (2018) 207-219.

[6] S. Prabhakar, A.S. Sekhar, A.R. Mohanty, Vibration analysis of a misaligned rotor-coupling-bearing system passing through the critical speed, J. Mech. Eng. Sci. 215 (12) (2001) 1417-1428.

[7] P.N. Saavedra, D.E. Ramirez, Vibration analysis of rotors for the identification of shaft misalignment, J. Mech. Sci. 218 (2004) 971-985.

[8] Z. Janusz, The analysis of the rotor's longitudinal vibration with large misalignment of shafts and rotex type coupling, Diagn. Struct. Health Monitor. 2 (2011) 19-23.

[9] Z.Y. Guan, P. Chen, X.Y. Zhang, et al., Vibration analysis of shaft misalignment and diagnosis method of structure faults for rotating machinery, Int. J. Perform Eng. 13 (2017) 337-347.

[10] M. Michael, V. Florian, V. Bram, The use of orbitals and full spectra to identify misalignment, Struct. Health Monitor. 5 (2014) 215-222.

[11] A.S. Sekhar, B.S. Prabhu, Effects of coupling misalignment on vibrations of rotating machinery, J. Sound Vib. 185 (4) (1995) 655-671.

[12] Z. Wan, J.P. Jing, G. Meng, et al., Non-linear dynamic behaviors and stability of a rotor-bearing system with flexible coupling misalignment, J. Vib. Shock 31 (2012) 20-25.

[13] M. Li, Z.G. Li, Theoretical and experimental study on dynamic of rotor-bearing system with the faults of coupling misalignment, J. Vib. Meas. Diagn. 35 (2015)345-351.

[14] G.Q. Feng, B.Z. Zhou, L.J. Lin, Misalignment analysis for support bearing in an inner-and-outer dual-rotor system, J. Vib. Shock 31 (2012) 142-147.

[15] Q.K. Li, M.F. Liao, Y.F. Jiang, The vibration features analysis of twin spool rotor with misalignment fault, Mech. Sci. Technol. Aerosp. Eng. 33 (2014) 1916-1920.

[16] A.M. Mikula, The Leading-Edge-Groove Tilting-Pad Thrust Bearing: Recent Developments, J. Tribol. 107 (1985) 423-428.

[17] N. Mitrovic, M. Milosevic, N. Momcilovic, A. Petrovic, Z. Miskovic, A. Sedmak, P. Popovic, Local Strain and Stress Analysis of Globe Valve Housing Subjected to External Axial Loading, Key Eng. Mater. 586 (2014) 214-217.

[18] V. Martsinkovsky, et al., Designing Thrust Sliding Bearings of High Bearing Capacity, Procedia Eng. 39 (2012) 148-156.

[19] S. Woo, D.L. O'Neal, Reliability design and case study of mechanical system like a hinge kit system in refrigerator subjected to repetitive stresses, Eng. Fail. Anal. 99 (2019) 319-329.

[20] R. Sepe, A. Greco, A. De Luca, E. Armentani, F. Berto, Experimental and FEM numerical assessment of multiaxial fatigue failure criteria for a rolling Stock's seats structure, Eng. Fail. Anal. 102 (2019) 303-317.

[21] G. Vukelic, G. Vizentin, Z. Bozic, L. Rukavina, Failure analysis of a ruptured compressor pressure vessel, Procedia Struct. Integrity 31 (2021) 28-32.

[22] A. Vazdirvanidis, G. Pantazopoulos, A. Louvaris, Failure analysis of a hardened and tempered structural steel (42CrMo4) bar for automotive applications, Eng. Fail. Anal. 16 (4) (2009) 1033-1038.

[23] M. Katinic, D. Kozak, I. Gelo, D. Damjanovic, Corrosion fatigue failure of steam turbine moving blades: A case study, Eng. Fail. Anal. 106 (2019).

[24] P. Wittke, et al., Mechanism-oriented characterisation of the load direction-dependent cyclic creep behavior of the magnesium alloys Mg-4Al-2Ba-2Ca and AE42 at room temperature, Eng. Fail. Anal. 103 (2019) 124-131.

[25] I. Camagic, Z. Burzić, S.A. Sedmak, A. Sedmak, D. Lazarevic, Integrity and Life Assessment Procedure for a Reactor, Procedia Struct. Integrity 18 (2019) 385-390.

[26] S. Papadopoulou, I. Pressas, A. Vazdirvanidis, G. Pantazopoulos, Fatigue failure analysis of roll steel pins from a chain assembly: Fracture mechanism and numerical modeling, Eng. Fail. Anal. 101 (2019) 320-328.

[27] D. Carlson, et al., The Effect of Bearing Steel Composition and Microstructure on Debris Dented Rolling Element Bearing Performance, SAE Int. Off-Highway Congress (2002) 330-338.

[28] G.A. Pantazopoulos, A Short Review on Fracture Mechanisms of Mechanical Components Operated under Industrial Process Conditions: Fractographic Analysis and Selected Prevention Strategies, Metals 9 (2019) 148.

[29] F. Ferroudji, Static Strength Analysis of a Full-scale 850 kW wind Turbine Steel Tower, Int. J. Eng. Adv. Technol. 8 (2019) 403-406.

[30] K. Monkova, M. Urban, P.P. Monka, S. Moravka, Z. Bozic, Design of the levers at the development of new self-equalising thrust bearings, Procedia Struct. Integrity 31 (2021) 92-97.

[31] Li, Junning et al., Thermal Elastohydrodynamic Lubrication Analysis of High-Speed and Light-Load Rolling Bearing with Double Rings Rotation, Technical Gazette, 29/1, 2022.

[32] S. Basu, A.K. Debnath, In Power Plant Instrumentation and Control Handbook (Second Edition), 2019, ISBN 9780081028049.

[33] Budynas R.G. (1999) Advanced Strength and Applied Stress Analysis, McGraw-Hill, ISBN 007116099X.

[34] Y. Ge, K. Wang, Effect of tempering temperature on precipitate evolution and mechanical properties of 34CrNiMo6 steel, Mater. Technol. 53 (4) (2019)527-534.

[35] M. Urban, K. Monkova, Research of Tribological Properties of 34CrNiMo6 Steel in the Production of a Newly Designed Self-Equalizing Thrust Bearing, Metals 10 (1) (2020) 84.

[36] S. Moravka, Calculation of properties of new bearings of Wikov test turbo gearbox. Influence of segment support stiffness. ALFA interim report. Research Report No. NTC-VYZ-12-117 for the Alfa project of the Technology Agency of the Czech Republic No. TA01011251, New Technologies - Research Center, University of West Bohemia, Pilsen, 2012.

[37] User and Reference Guide for the Intel® Fortran Compiler 14.0, Intel Corporation, 2200 Mission College Blvd., Santa Clara, CA 95054-1549, USA, 2013.

[38] H. Hertz, Miscellaneous Papers (translated by Jones, D.E., and Scott, D.A.), Macmillian and Co., Ltd., London, 1896, pp. 146-193. (Contains English translation of the papers from Journal Reine und angewandte Mathematik (Crelle), Vol. 92, 1881, pp. 156-171 and Verhand Vereins Beforder Gewerbefleisses, Nov. 1882).

[39] H. Hertz, Uber die Beruhrung fester elastischer Korper, Journal fur die reine und angewandte Mathematik 92, 156-171, Berlin, 1881.

[40] B. Savić et al., Implementation of a Non-Linear Regression Model in Rolling Bearing Diagnostics, Technical Gazette, 29/1, 2022.

[41] P. Spiros Pantelakis, G. Pantazopoulos, A. Toulfatzis, A. Vazdirvanidis, A. Rikos, Engineering approaches in industry: Accelerated carbide tool wear failure during machining of hot work hardened tool steel: A case study, Int. J. Struct. Integrity 6 (2) (2015) 290-299.

[42] F. Iacoviello, V. Di Cocco, E. Franzese, S. Natali, High temperature embrittled duplex stainless steels: influence of the chemical composition on the fatigue crack propagation, Procedia Struct. Integrity 3 (2017) 308-315.

[43] T. Smolnicki, M. Stanco, D. Pietrusiak, Distribution of loads in the large size bearing - problems of identification, Technical Gazette, 20/5, 2013.

[44] P.K. Adishesha, Effect of Steel Making and Processing Parameters on Carbide Banding in Commercially Produced ASTM A-295 52100 Bearing Steel, in Bearing Steel Technology, 2002, pp. 27-46.